PERGAMON

International Journal of Solids and Structures 40 (2003) 4097–4106

INTERNATIONAL JOURNAL OF SOLIDS and STRUCTURES

www.elsevier.com/locate/ijsolstr

Buckling of rectangular plates subjected to nonlinearly distributed in-plane loading

Charles W. Bert *, Krishna K. Devarakonda *

School of Aerospace and Mechanical Engineering, The University of Oklahoma, 865 Asp Av., Room 212, Norman, OK 73019-1052, USA

Received 14 February 2003; received in revised form 14 February 2003

Abstract

The problem of buckling of a rectangular plate subjected to uniformly distributed in-plane compressive loading at each end goes back to the work of Bryan in 1890–91. The same problem, for the case of linearly varying in-plane compressive loading at each end, was first treated by several European investigators about 90 years ago. The case of loading that is nonlinearly distributed along two opposite plate edges is considerably more complicated in that it requires that first the plane elasticity problem be solved to obtain the distribution of in-plane stresses. Then the buckling problem must be solved. This problem was claimed to have been solved by van der Neut in 1958 for a half-sine load distribution and later by Benoy for a parabolic distribution. However, their work was based on an incorrect in-plane stress distribution. Here is presented a solution for the half-sine load distribution on two opposite sides, based on a more realistic in-plane stress distribution. This distribution shows a decrease (diffusion) in axial stress as the distance from the loaded edges is increased. The buckling loads are calculated using Galerkin method and the results are compared with the inaccurate results in the literature.

Keywords: Buckling; Galerkin method; Nonlinearly distributed load; Rectangular plates; Superposition method

1. Introduction

The problem of buckling of a rectangular elastic plate subjected to in-plane compressive or shear loading is important in the shipbuilding, aircraft, and automotive industries. The first work in this area was due to Bryan (1890–91) (see Timoshenko and Gere, 1961, p. 351). Bryan considered the case of uniformly distributed compressive loading and all four edges simply supported. The cases of more complicated boundary conditions have been solved by innumerable investigators through the years.

The case of linearly varying edge loading was first considered independently in 1910 by Timoshenko and in 1914 by Boobnov, using approximate methods (see Timoshenko and Gere, 1961, p. 373). This loading case was also analyzed, using approximate methods, by Way (1936), Favre (1948), Grossman (1949),

* Corresponding authors. Tel.: +1-405-325-1736 (C.W. Bert), +1-405-325-9835 (K.K. Devarakonda); fax: +1-405-325-1088.
E-mail addresses: cbert@ou.edu (C.W. Bert), kk_d28@yahoo.com (K.K. Devarakonda).

0020-7683/03/$ - see front matter © 2003 Elsevier Science Ltd. All rights reserved.
doi:10.1016/S0020-7683(03)00205-1

Noel (1952), McKenzie (1964), and Dawe (1969). Recently, Leissa and Kang (2001) and Kang and Leissa (2001) solved this same problem exactly in a series sense.

There have been very few previous solutions for the case of nonlinearly distributed edge loadings. Perhaps this scarcity is due to the additional complexity of having to first solve for the internal prestress distribution as a problem in plane-stress elasticity. The first work in this area was due to van der Neut (1958), who considered a uniaxial compressive loading with a half sine distribution. The work of Benoy (1969) should also be mentioned. He considered a uniaxial compressive loading with a parabolic distribution and obtained an energy solution.

It should be pointed out that the works of van der Neut (1958) and Benoy (1969) both suffered from these serious deficiencies:

- The x-direction in-plane normal stress distribution was tacitly assumed to depend only on the y-position coordinate. (In actuality there is a stress-diffusion phenomenon which causes this stress distribution to vary with x as well as y.)
- The contributions of the y-direction in-plane normal stress distribution and the in-plane shear stress distribution have been ignored.
- It was assumed that the buckled waveform and thus the bending strain energy for the nonuniform-loading case is identical to that for uniform loading.

The goal of the present work is to remove these deficiencies and thus to achieve more accurate results for the buckling load.

2. Preliminary considerations

The problem geometry and coordinate system are shown in Fig. 1. The first approach investigated here was to use the polynomial form of the Airy stress function, systematized by Niedenfuhr (1957) and Neou (1957). The resulting distributions of in-plane stresses satisfied compatibility, vanishing shear stresses on all four edges, and the parabolically distributed loading on the edges at $x = \pm a/2$. Unfortunately, it was not possible to satisfy the conditions of vanishing normal stresses on the edges $y = \pm b/2$. However, it was possible to have the resultant force

$$F_y = \int_{-a/2}^{a/2} h\sigma_y \, \mathrm{d}x$$

vanish at $y = \pm b/2$. Here h is the plate thickness. Nevertheless, the maximum value of σ_y at $y = \pm b/2$ was $(-2/3)(a/b)^2\sigma_0$, where σ_0 is the maximum value of the parabolically distributed σ_x at $x = \pm a/2$. It is clear that the maximum value of σ_y is not negligible relative to the maximum value of σ_x except for very short (low aspect ratio) plates.

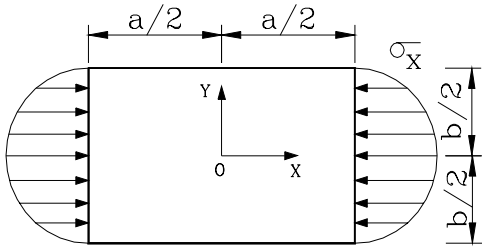

Fig. 1. Geometry and loading of the plate.

In view of the inaccuracy of the Niedenfuhr–Neou prebuckling results, it was decided to use a direct Fourier series approach using the superposition method (see Timoshenko and Goodier, 1970; Gorman and Singhal, 1993).

3. In-plane stress solution

3.1. Theory

As shown in Fig. 1 a rectangular plate with the coordinate system placed at the center of the plate is loaded with the in-plane loading as

$$\sigma_x = \sigma_0 \cos(\pi y/b) \tag{1}$$

applied at the edges $x = \pm a/2$. Substituting the Airy stress function ϕ_1 given by

$$\phi_1 = f(x)\cos(\pi y/b) \tag{2}$$

into the governing differential equation $\nabla^4\phi = 0$, one can obtain the general solution for the functional $f(x)$ as

$$f(x) = C_1 \cosh\left(\frac{\pi x}{b}\right) + C_2 \sinh\left(\frac{\pi x}{b}\right) + C_3 x \cosh\left(\frac{\pi x}{b}\right) + C_4 x \sinh\left(\frac{\pi x}{b}\right) \tag{3}$$

in which C_1 through C_4 are constants which are to be obtained from the boundary conditions. It is to be noted that the stress function solution as given by Eqs. (2) and (3) gives a zero normal stress at $y = \pm b/2$ edges.

Substituting the zero shear stress boundary condition as well as the normal stress distribution as defined in Eq. (1), at the edges $x = \pm a/2$, yields a complete solution for the in-plane stresses. (See Appendix A for the complete solution.)

$$\phi_1 = \left(C_1 \cosh\left(\frac{\pi x}{b}\right) + C_4 x \sinh\left(\frac{\pi x}{b}\right)\right)\cos\left(\frac{\pi y}{b}\right) \tag{4}$$

However, the above in-plane stress solution gives a residual shear stress distribution at the $y = \pm b/2$ edges which can be eliminated using a superposed Fourier solution as discussed by Timoshenko and Goodier (1970) and by Gorman and Singhal (1993). In the present problem, a solution consisting of two superposed stress functions is sufficient to satisfy the required boundary conditions accurately.

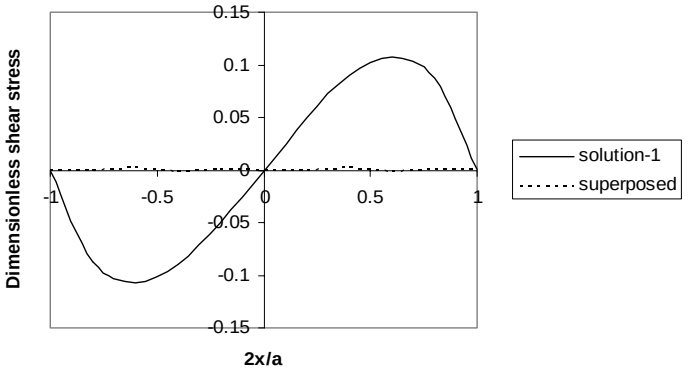

Fig. 2. Dimensionless shear stress (τ_{xy}/σ_0) distribution at ($2y/b = \pm 1$) edges (aspect ratio $a/b = 1$) (solution-1 corresponds the stress function solution ϕ_1 and superposed solution is the total ($\phi_1 + \phi_2$) solution).

The stress function solution in Eq. (4) produces a shear stress distribution in the x-direction which can be easily expanded as a Fourier sine series. In order to eliminate these shear stresses, one can start with a second stress function solution, which produces sinusoidal shear stress distribution in the x-direction. After eliminating the unsymmetric components, this stress function is given by

$$\phi_2 = \sum_{m=1,2,\ldots} \left(D_{1m} \cosh\left(\frac{2m\pi y}{a}\right) + D_{4m} y \sinh\left(\frac{2m\pi y}{a}\right)\right) \cos\left(\frac{2m\pi x}{a}\right) \tag{5}$$

Imposing the zero normal stress boundary condition at the $y = \pm b/2$ edges, an interrelation between D_{1m} and D_{4m} can be obtained. Now superposition of the shear stress distribution at the $y = \pm b/2$ edges and equating the resultant to zero yields a complete solution.

It is to be observed that whereas the initial stress-function solution (ϕ_1) is a one-term solution, the second stress-function solution (ϕ_2) is a series solution. However, at the most the first three or four series terms are sufficient to obtain a close approximation for the residual shear stress distribution due to ϕ_1.

Although the stress-function solution ϕ_2 has zero normal stresses at the $y = \pm b/2$ edges and zero shear stresses at $x = \pm a/2$ edges, it does produce a residual normal stress (σ_x). However, it is observed that this σ_x stress distribution is once again sinusoidal with a very small magnitude. Consequently, a renormalization of the superposed σ_x distribution has to be carried out such that the resulting σ_x stresses are very nearly as specified by Eq. (1). This renormalization is carried out using a small uniform stress and a multiplication factor. This methodology gives good results as shown in the next section.

In using the two-stress-function solution, however, one can observe that it deviates from the superposition method as developed by Timoshenko and used extensively by Gorman. For the present problem, the superposition method requires a four stress function solution wherein each stress function has to have enough terms to obtain satisfactory convergence. From a preliminary analysis, it is concluded that the superposition method showed a slow convergence for σ_y residual stress removal (at the $y = \pm b/2$ edges). Moreover the resulting in-plane stress distribution is considerably complicated and the in-plane stress boundary conditions are approximately satisfied. Therefore in the present analysis, the two-stress-function approach is carried out.

3.2. Numerical results for in-plane stress distribution

Fig. 2 shows the comparative shear stresses at $y = \pm b/2$ plate edges for the case of ϕ_1 stress function solution only and the superposed ($\phi_1 + \phi_2$) stress function solution. From this figure, one can clearly see that the superposed solution satisfied the zero shear stress boundary condition (on all four edges) very accurately.

The direct Fourier solution (two-stress-function solution) in the present analysis shows a rapid reduction (or diffusion) of σ_x—in-plane stresses towards the center of the plate. This decrease is more pronounced at higher plate aspect ratios (Figs. 3 and 4). Such diffusion of in-plane stresses was ignored in the work of van der Neut (1958) and Benoy (1969). In the absence of such diffusion, the applicability of those solutions is very much restricted to small plate aspect ratios. (More will be discussed in Section 4.2 when the buckling solution is presented.)

Fig. 3 shows the normal (σ_x) stress distribution across the plate width at various plate sections and in Fig. 4 the in-plane normal stress at $2y/b = 0$, and shear stress at $2y/b = 0.5$, are plotted along the plate half length. These figures show the normal stress diffusion from the edges of the plate towards the center of the plate. At higher aspect ratios, the nonlinearity of the in-plane stress (σ_x) is significant only at a distance up to the first quarter from the plate edge approximately and thereafter the in-plane stress essentially remains uniform (see $2x/a = 0$ and $2x/a = 0.5$ curves in Fig. 3). Also Fig. 4 shows that the maximum shear stress moves toward the plate edge as the aspect ratio is increased. Consequently the effect of in-plane shear stress

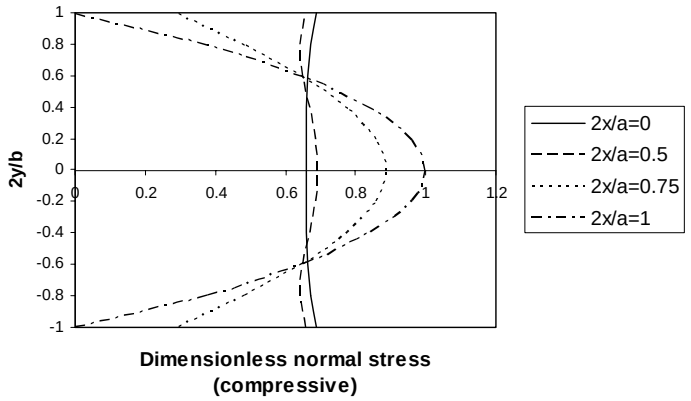

Fig. 3. Normal stress ($-\sigma_x/\sigma_0$) distribution at stations $2x/a = 0$, 0.5, 0.75, 1.0 (aspect ratio $a/b = 3$).

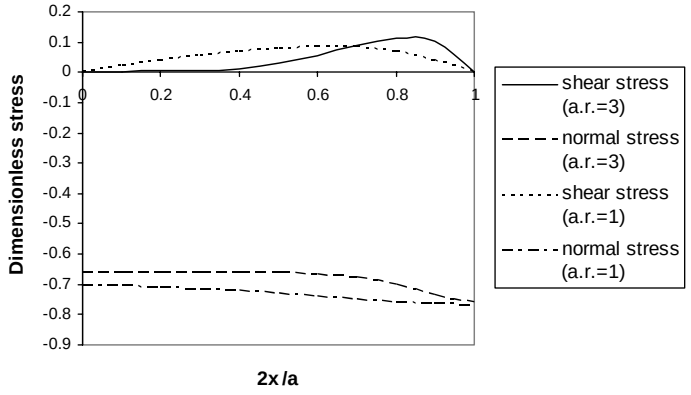

Fig. 4. Dimensionless normal stress (σ_x/σ_0) at $2y/b = 0$ and shear stress (τ_{xy}/σ_0) at $2y/b = 0.5$, across plate half length (a.r. = aspect ratio).

on buckling at high plate aspect ratios reduces. One can notice from Fig. 4 that for lower plate aspect ratios, the stress diffusion rate is small compared to those plates of high aspect ratios.

In order to see the normal stress diffusion more clearly, a three dimensional plot of the dimensionless normal stress (compressive) is shown in Fig. 5 for a plate aspect ratio of 3. In this plot, the z-coordinate is the normal stress magnitude corresponding to the (x, y) location of the plate. From this figure one can see the rapid normal stress diffusion from $2x/a = \pm 1$ edges towards the center of the plate.

Fig. 6 shows the resultant shear stress variation across plate width at various plate sections. The maximum magnitude of shear stress increases from the middle of the plate towards the plate edges and then reduces to zero at the plate edges (see Fig. 4 also). From the equilibrium perspective, this rapid increase in shear stress corresponds to the normal stress diffusion.

The in-plane stress solution in the present analysis show that:

- In general all the in-plane stresses are functions of both x and y.
- The in-plane normal stress in the x-direction changes from a half sinusoidal distribution at the plate edges to uniform (approximately) towards the plate center. This stress diffusion is more prominent at high plate aspect ratios.

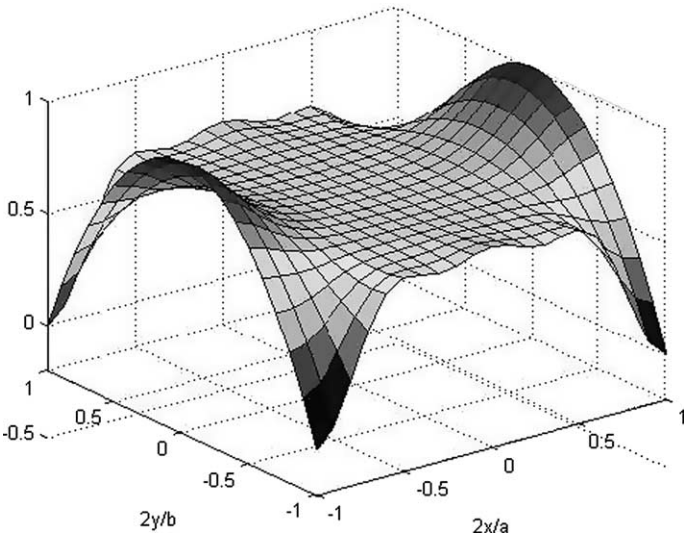

Fig. 5. Dimensionless normal stress (σ_x/σ_0) versus position in the midplane of the plate (aspect ratio = 3).

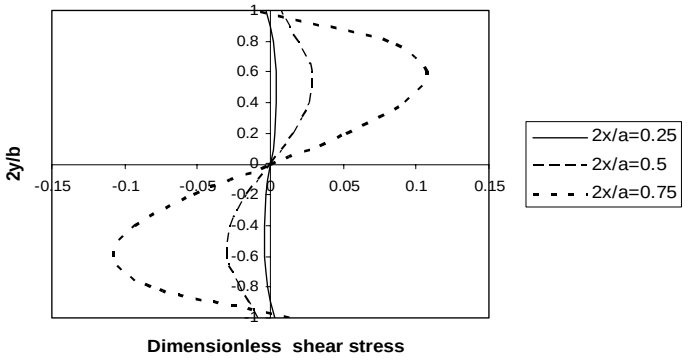

Fig. 6. Shear stress (τ_{xy}/σ_0) distribution across plate width (aspect ratio = 3).

- The normal stress in the *y*-direction and the shear stress distributions are significant and are highly non-linear.

4. Buckling solution

4.1. Theory

The governing differential equation for thin plate buckling is

$$\nabla^4 w + \frac{h}{D}\left(\sigma_x \frac{\partial^2 w}{\partial x^2} + 2\tau_{xy}\frac{\partial^2 w}{\partial x\,\partial y} + \sigma_y \frac{\partial^2 w}{\partial y^2}\right) = 0 \tag{6}$$

where D is the flexural rigidity, h is the plate thickness, and w is the normal deflection.

Owing to the complexity of the resulting plate buckling equation when each of the in-plane stress is a series sum, exact analytical solution may not be possible. Therefore, the buckling solution is obtained by using the Galerkin method for the case of simply supported rectangular plates. For the present case of simply supported rectangular plates with central coordinate system the trial functions are

$$w(x,y) = w_0 \cos(m\pi x/a)\cos(n\pi y/b), \quad \{m,n = 1,3,5,\ldots\}$$

Numerical calculations were conducted using symbolic math package Mathematica (version 4.0).

4.2. Numerical results for buckling

Numerical computations are done using the first four trial functions. Numerical results are compared for convergence between three-term Galerkin solution and four-term solution. Up to three significant digit accuracy was obtained for all buckling loads with the four-term solution. Some representative results for dimensionless buckling loads are presented in Table 1 and the dimensionless buckling coefficient for various plate aspect ratios is plotted in Fig. 7. Although the results obtained by Benoy (1969) are for the case of parabolic loading, one can compare the solutions due to the close similarity of sinusoidal and parabolic stress distributions.

The buckling loads in the present analysis are higher than those of Benoy's results. The reasons for this can be explained by the following reasoning. In the present analysis, the in-plane stress solution contains both σ_y normal stress and τ_{xy} shear stresses which were neglected previously. Moreover, the σ_x stress distribution shows the stress diffusion from the loaded edge towards the middle of the plate. As a result, the maximum stress is reduced (see Fig. 3) and stresses near the edges $2y/b = \pm 1$ are increased. As the plate

Table 1
Buckling coefficient for various aspect ratios[a]

α	Dimensionless buckling coefficient K		
	Present solution (four term Galerkin) (sinusoidal)	Benoy (parabolic)	van der Neut (sinusoidal)
0.5	7.841	7.08	–
1	5.146	4.59	4.68
3	5.748	4.53	–

[a] Here $\alpha = a/b$, and $K = \sigma_0 hb^2/\pi^2 D$.

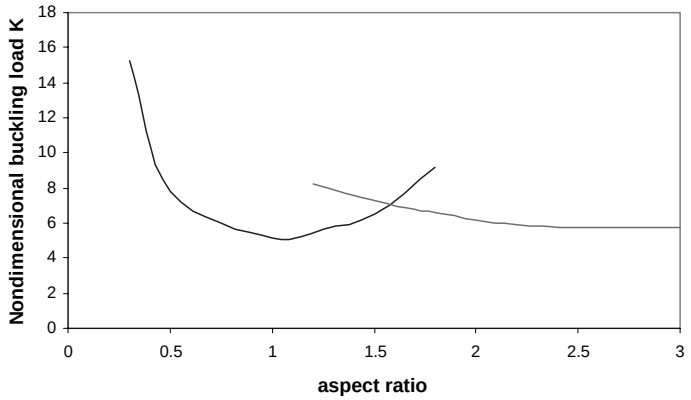

Fig. 7. Nondimensional buckling load ($\sigma_0 hb^2/\pi^2 D$) for various plate aspect ratio (α).

edges are supported, this stress increase near the edges would cause the plate to sustain higher buckling loads. As the stress diffusion is higher at higher plate aspect ratios (Figs. 4 and 5) the buckling loads are progressively higher at higher plate aspect ratios. This is clearly evident from Table 1 (and also from Fig. 7) that the percentage difference between the present solution and Benoy solution increased from about 10% at $\alpha = 0.5$ to more than 26% at $\alpha = 3$. It is interesting to note from Fig. 7, that up to the plate aspect ratio of 3 only the first two buckling modes are active as against three buckling modes in Benoy's results.

5. Concluding remarks

An analytical solution for buckling of simply supported rectangular plates subjected to sinusoidal in-plane compressive stress distribution at each end is presented as a superposed Fourier solution. The resulting in-plane stress solution consists of two normal stresses (x, y directions) and a shear stress which are nonlinearly distributed throughout the plane of the plate. The in-plane stress distribution in the present solution shows a decrease (diffusion) in axial stress (σ_x) as the distance from the loaded edges is increased. At high plate aspect ratios, this stress diffusion is more rapid and it remains essentially uniform at a reduced value for most part of the plate. This stress diffusion is in accord with Saint–Venant's principle and is believed to be a more accurate description of the sinusoidal edge loading. It is observed that similar to the normal stress diffusion, the maximum shear stress location moved towards plate edges at higher plate aspect ratios causing the shear stress to be more effective towards resisting buckling. As a consequence, present analysis shows increased buckling loads at higher plate aspect ratios than those obtained in the literature. It is also observed that up to the plate aspect ratio of 3.0, only the first two buckling modes are active. The dimensionless buckling load for various plate aspect ratios shows a qualitative agreement with the existing plate buckling literature.

Acknowledgements

The authors acknowledge helpful discussions with Professors Arthur Leissa and Daniel Gorman.

Appendix A. Complete in-plane solution

The first terms of the stress distributions are

$$\sigma_{x1} = -\frac{\pi^2}{b^2}\left(C_1 \cosh\left(\frac{\pi x}{b}\right) + C_4 x \sinh\left(\frac{\pi x}{b}\right)\right)\cos\frac{\pi y}{b} \tag{A.1}$$

$$\sigma_{y1} = \left(\left(C_1\frac{\pi^2}{b^2} + C_4\frac{2\pi}{b}\right)\cosh\frac{\pi x}{b} + C_4\frac{\pi^2}{b^2}x\sinh\frac{\pi x}{b}\right)\cos\frac{\pi y}{b} \tag{A.2}$$

$$\tau_{xy1} = \frac{\pi}{b}\left(\left(C_1\frac{\pi}{b} + C_4\right)\sinh\frac{\pi x}{b} + C_4\frac{\pi}{b}x\cosh\frac{\pi x}{b}\right)\sin\frac{\pi y}{b} \tag{A.3}$$

where

$$C_1 = \frac{\frac{\pi a}{2b}\cosh\left(\frac{\pi a}{2b}\right) + \sinh\left(\frac{\pi a}{2b}\right)}{\frac{\pi a}{2b} + \sinh\left(\frac{\pi a}{2b}\right)\cosh\left(\frac{\pi a}{2b}\right)}\frac{\sigma_0 b^2 h}{\pi^2} \tag{A.4}$$

$$C_4 = -\frac{\frac{\pi a}{2b}\sinh\left(\frac{\pi a}{2b}\right)}{\frac{\pi a}{2b} + \sinh\left(\frac{\pi a}{2b}\right)\cosh\left(\frac{\pi a}{2b}\right)}\frac{\sigma_0 b^2 h}{\pi^2} \tag{A.5}$$

The second terms of the stress distributions are

$$\sigma_{x2} = \sum_{m=1,2,\ldots} \frac{4m^2\pi^2}{a^2}\left[\left(D_{1m} + \frac{a}{4m\pi}D_{4m}\right)\cosh\left(\frac{2m\pi y}{a}\right) + D_{4m}y\sinh\left(\frac{2m\pi y}{a}\right)\right]\cos\left(\frac{2m\pi x}{a}\right) \tag{A.6}$$

$$\sigma_{y2} = -\sum_{m=1,2,\ldots} \frac{4m^2\pi^2}{a^2}\cos\left(\frac{2m\pi x}{a}\right)\left[D_{1m}\cosh\left(\frac{2m\pi y}{a}\right) + D_{4m}y\sinh\left(\frac{2m\pi y}{a}\right)\right] \tag{A.7}$$

$$\tau_{xy2} = \sum_{m=1,2,\ldots} \frac{4m^2\pi^2}{a^2}\sin\left(\frac{2m\pi x}{a}\right)\left[\left(D_{1m} + D_{4m}\frac{a}{2m\pi}\right)\sinh\left(\frac{2m\pi y}{a}\right) + D_{4m}y\cosh\left(\frac{2m\pi y}{a}\right)\right] \tag{A.8}$$

where

$$D_{1m}\cosh\frac{m\pi b}{a} + D_{4m}\sinh\frac{m\pi b}{a} = 0 \tag{A.9}$$

let

$$\tau_1 = \frac{\pi}{b}\left(\left(C_1\frac{\pi}{b} + C_4\right)\sinh\frac{\pi x}{b} + C_4\frac{\pi}{b}x\cosh\frac{\pi x}{b}\right) \tag{A.10}$$

and

$$F_{1n} = \int_{-1}^{1} \tau_1 \sin\frac{2n\pi x}{a}\,\mathrm{d}x \quad (n = 1, 2, 3, \ldots) \tag{A.11}$$

$$D_{1m} = \frac{-F_{1m}a^2}{4m^2\pi^2\left(1 - \dfrac{1}{2m\pi\tanh((m\pi b)/a)}\right)\sinh\dfrac{m\pi b}{a} - \dfrac{1}{\tanh((m\pi b)/a)}\dfrac{b}{2}\cosh\dfrac{m\pi b}{a}} \tag{A.12}$$

$$D_{4m} = -\frac{D_{1m}}{\tanh\dfrac{m\pi b}{a}} \tag{A.13}$$

References

Benoy, M.B., 1969. An energy solution for the buckling of rectangular plates under non-uniform in-plane loading. Aeronautical Journal 73, 974–977.

Bryan, 1890–91. On the stability of a plane plate under thrusts in its own plane, with applications to the "buckling" of the sides of a ship. Proceedings of the London Mathematical Society 22, 54–67.

Dawe, D.J., 1969. Application of the Discrete Element Method to the Buckling Analysis of Rectangular Plates under Arbitrary Membrane Loading. The Aeronautical Quarterly 20, 114–128.

Favre, H., 1948. The influence of its own weight on the stability of a rectangular plate. In: Proceedings of 7th International Congress of Applied Mechanics, London, vol. 1. pp. 151–159.

Gorman, D.J., Singhal, R.K., 1993. A superposition-Rayleigh–Ritz method for free vibration analysis of non-uniformly tensioned membranes. Journal of Sound and Vibration 162 (3), 489–501.

Grossman, N., 1949. Elastic stability of simply supported flat rectangular plates under critical combinations of transverse compression and longitudinal bending. Journal of the Aeronautical Sciences 16, 272–276.

Kang, J.H., Leissa, A.W., 2001. Vibration and buckling of SS–F–SS–F rectangular plates loaded by in-plane moments. International Journal of Structural Stability and Dynamics 1, 527–543.

Leissa, A.W., Kang, J.H., 2001. Exact solutions for the free vibrations and buckling of rectangular plates with linearly varying in-plane loading. In: Proceedings, 2001 ASME International Mechanical Engineering Congress and Exhibition, New York. ASME Paper IMECE2001/AD-23758.

McKenzie, K.I., 1964. The buckling of a rectangular plate under combined biaxial compression, bending and shear. Aeronautical Quarterly 15, 239–246.

Neou, C.Y., 1957. A direct method for determining Airy polynomial stress functions. ASME Journal of Applied Mechanics 24, 387–390.

Niedenfuhr, F.W., 1957. On choosing stress functions in rectangular coordinates. Journal of Aeronautical Sciences 24, 460–461.

Noel, R.G., 1952. Elastic stability of simply supported flat rectangular plates under critical combinations of longitudinal bending, longitudinal compression, and lateral compression. Journal of the Aeronautical Sciences 19, 829–834.

Timoshenko, S.P., Gere, J.M., 1961. Theory of Elastic Stability, second ed McGraw-Hill Inc., New York.

Timoshenko, S.P., Goodier, J.N., 1970. Theory of Elasticity, third ed McGraw-Hill Inc., New York.

van der Neut, A., 1958. Buckling caused by thermal stresses. In: High temperature effects in aircraft structures. AGARDograph, No. 28, pp. 215–247.

Way, S., 1936. Stability of rectangular plates under shear and bending forces. ASME Journal of Applied Mechanics 3, A131–A135.